

2D BAO vs 3D BAO: Hints for new physics?

Ruchika¹ *

¹*Physics Department and INFN, Università di Roma “La Sapienza”, Ple Aldo Moro 2, 00185, Rome, Italy*

Accepted XXX. Received YYY; in original form ZZZ

ABSTRACT

In the era of tensions, when precision cosmology is blooming, numerous new theoretical models are emerging. However, it’s crucial to pause and question the extent to which the observational data we rely on are model-dependent. In this work, we study the comoving position of the acoustic peak, a cornerstone standard ruler in cosmology. We considered BAO observational datasets from two distinct teams and calculated the product hr_d with the help of each BAO data set along with SN I-a data from the Pantheon Plus sample. Our conclusion at present is that 2D and 3D BAO datasets are compatible with each other. Considering, no systematics in BAO, interpreting $\Omega_{m0} - hr_d$ plane may require physics beyond Λ CDM not just while using observational BAO data but also while observing it.

Key words: Baryon Acoustic Oscillations, Cosmological Tensions, Absolute Magnitude SNe I-a

1 INTRODUCTION

Since the pivotal supernova (SN) discovery of 1997, indicating the onset of the accelerated phase of the universe, cosmologists have diligently pursued measurements of cosmic expansion utilizing various observational probes. Notably, the cosmic microwave background (CMB) (Ade et al. 2016a,b; Aghanim et al. 2018), Type Ia supernovae (SN Ia) (Betoule et al. 2014; Perlmutter et al. 1997; Riess et al. 1998), and Baryon Acoustic Oscillations (BAO) (Beutler et al. 2011, 2012; Blake et al. 2012; Lauren et al. 2013, 2014) have emerged as key instruments for gauging the Hubble expansion or Hubble Constant. Precision cosmology hinges upon the accurate calibration and interpretation of observational data obtained from diverse probes, including the CMB and the standard distance ladder. Anomalies within these datasets have garnered significant attention, as they may herald breakthroughs in our understanding of fundamental cosmological processes.

Despite general agreement among most probes within a two to three-sigma range, recent analyses, particularly the Planck 2018 (Aghanim et al. 2018) and SH0ES 2022 datasets (Riess et al. 2022), have revealed tensions exceeding five sigmas. Several works have been dedicated to careful examination of CMB sky and standard distance ladder.

Hubble Hunter’s Guide (Knox et al. 2020) lists out many departures from Λ CDM to solve the cosmological tensions and singles out a solution which increases Hubble expansion rate before recombination by modifying sound horizon at drag epoch r_d . Other efforts have been made to identify anomalies in CMB polarization data (Matteo et al. 2023) with the help of JWST datasets. Studies like G-Transition hypothesis (Ruchika et al. 2022), Planck Mass transition (Kable et al. 2023) assess the requisite signatures within the standard distance ladder. By dissecting the underlying assumptions and methodologies, these studies seek to contextualize these anomalies within the broader framework of precision cosmology.

We recall that Baryon acoustic oscillations are considered to be one of the most powerful probes for measuring the undergoing phase of accelerated expansion of the universe. When combined with the Planck satellite results, one finds that the Universe is spatially flat (Aghanim et al. 2018). However, we stress that the traditional methods or the official BAO distances have an injection of cosmological information while estimating distances and the standard assumptions hold only for models that are not too dissimilar from Λ CDM (Thepuriya & Lewis 2015). This may be the serious limitation of the standard BAO approach and therefore while using them to quantify tensions among various cosmological probes, one needs to be very cautious. For BAO to infer cosmological distance and later use them to understand the fundamentals of our universe, estimates should be as much as possible model-independent, allowing one to perform multiple consistency checks of data and theory. It is still unclear if we can use all sorts of exotic models such as Ruchika et al. (2022); Kable et al. (2023); Dutta et al. (2020) to infer cosmological distances from standard BAO observations.

Recent solutions such as the Purely-Geometric-BAO (Anselmi et al. 2024) avoid the undesired injection of cosmological information into distances inferred from the BAO and may work better for studying cosmological tensions. Such analyses are particularly relevant in light of the current cosmological tensions.

In this work, we will analyze anomalies within Baryon Acoustic Oscillations. Before questioning the 6-parameter standard model of cosmology like everyone else, we address the question of how standard are the measurements for the standard ruler i.e. Baryon Acoustic Oscillations. We compared two different datasets from BAO. We argue that using different datasets to estimate cosmological information from the standard ruler should not bring significant change in the final inference of cosmological parameters. Keeping the model fixed to the simplest Λ CDM model, we focused on the inherent tensions between BAO measurements. This paper scrutinizes the discordance among two independent BAO datasets and explores the implications for our understanding of cosmic expansion. We also incorporated the SN-Ia dataset in our study. Taking just low redshift

* e-mail: ruchika.ruchika@roma1.infn.it

observational probes like SN I-a, we question here if BAO can be used as a model-independent probe to study the evolution of the universe and if it can be at all used to check different exotic models that are being proposed to solve cosmological tensions.

This paper is organized as follows. In section 2 we briefly review the physics of the BAOs. We describe the data used and the method of SNe calibration in section 3. We also discuss that standard BAO distance measurements are obtained through fitting approaches where cosmological parameters were kept fixed to a fiducial flat- Λ CDM cosmological model or by building the whole data analysis pipeline with flat- Λ CDM survey mocks and Nbody simulations close to the Planck best-fit cosmology. Results comparing 2D and 3D datasets are given in section 4. And, we put our comments on Early Dark Energy in section 5. In section 6, We incorporated the analysis with the DESI dataset. Section 7 is where we have an overall discussion of BAO 2D, BAO 3D and DESI BAO Dataset. In section 8, we conclude the final remarks.

2 BARYON ACOUSTIC OSCILLATION AS A STANDARD RULER

Baryon Acoustic Oscillations (BAO) serve as a crucial cosmological standard ruler in the field of cosmology. They provide valuable information for understanding the large-scale structure of the universe and inferring cosmological parameters from observational data. The comoving position of the acoustic peak, which is a characteristic feature of the BAO, is particularly targeted by the cosmological community. This peak arises as a result of acoustic waves travelling through the early universe, leaving a distinct imprint on the distribution of matter. By measuring the characteristic scale of these oscillations in the large-scale structure of the universe, researchers can use BAO as a standard ruler to infer cosmological parameters such as the expansion rate of the universe and the amount of dark energy. In essence, BAO offers a powerful tool for cosmologists to probe the underlying cosmology of the universe by studying the clustering of galaxies and other cosmic structures. This allows them to better understand the nature of dark energy, dark matter, and the overall geometry and evolution of the universe.

In the standard cosmological description, in the early universe before the recombination epoch, baryons and photons were tightly coupled to each other and there was a formation of acoustic waves within the primordial photon-baryon plasma. As the universe expanded and cooled, reaching the epoch of decoupling, known as the drag epoch, the propagation of these acoustic waves ceased. At this pivotal moment, the baryon distribution retained imprints of the acoustic oscillations, manifesting as overdensities separated by a distinct length scale ($r_d \sim 150$ Mpc) known as the sound-horizon comoving length at the drag epoch. As this signature imprinted on matter distribution is governed by early universe physics before and around recombination, it is treated as a standard ruler. In fact, it is also well calibrated by CMB observations to very high accuracy (Aghanim et al. 2018). Similarly, Eisenstein & Hu (1998) found a bAO peak in large-scale correlation function around the same comoving galaxy separation ($100 h^{-1}$) Mpc. And that is why BAO is used to constrain dark energy behaviour and helps in breaking the residual degeneracies with CMB observations.

The evolution of matter on large scales, including dark matter and baryons, is primarily influenced by gravity. This gravitational interaction leaves a distinctive feature in the 2-point correlation functions (CF) of matter and its observed tracers, such as galaxies. This char-

acteristic scale, a consequence of the physics governing the early universe, serves as a fundamental cosmological standard ruler.

Since the so-called acoustic peak was very closely identified with the correlation function (CF) feature in BAO, it sparked the initial notion of measuring a comparable length scale across both the early and late universe. The intention behind this approach was to leverage the consistency of this scale throughout cosmic history, thereby harnessing its cosmological implications. However, in the present era of precision cosmology, this excellent intuition is encountering several challenges.

We now evidently know that the primordial sound horizon at drag epoch r_d estimated from Cosmic Microwave Background is cosmological model dependent and depends on the modelling of late-time physics. On the other hand, while calculating the r_d from late-time physics, one needs to model scale-dependent galaxy bias in galaxy correlation function non-linearities which can be time as well as model-dependent.

To fit the observational anisotropic power spectrum data from CMB sky, we mostly assume a standard cosmological model (e.g. flat Λ CDM), and we can calculate the value of r_d as the derived parameter. Using late-time probes such as the galaxy correlation function, r_d needs to be derived again from cosmology-dependent multi-parameter fit.

2.1 Parameterizing the Comoving Distance Scale

Using late-time probes, there are two ways of utilising the 2-point correlation function to determine the BAO feature in literature. One is via two-point correlation (3D BAO Dataset) (Alam et al. 2016) $\xi(s)$ in configuration and Fourier space and the other is using 2-point angular correlation function (2D BAO Dataset) (Carvalho et al. 2016) $\omega(\theta)$ where s and θ are comoving radial and angular separation respectively. Below we describe both of them in detail.

2.1.1 Two Point Correlation Function

Among several 3D estimators in literature, the most commonly used is the Two Point Correlation Function (2PCF)

$$\xi(s) = \frac{DD(s) - 2DR(s) + RR(s)}{RR(s)}, \quad (1)$$

where DD(s) and RR(s) represent the number of galaxy pairs in real and random-random catalogues respectively. The comoving distance s is chosen assuming a fiducial cosmology. The comoving distance between two galaxies at redshift z_1 and z_2 is given by

$$s = \sqrt{r^2(z_1) + r^2(z_2) - 2r(z_1)r(z_2)\cos\theta_{12}}, \quad (2)$$

where θ_{12} is the angular distance between pair of galaxies at redshift z_1 and z_2 . Choosing the expression for r is what makes it cosmological model dependent. For flat Λ CDM, H_0 and Ω_m being the Hubble parameter at present and matter density parameter, r is expressed as:

$$r(z_i) = \frac{c}{H_0} \int_0^{z_i} \frac{dz}{\sqrt{\Omega_m(1+z)^3 + (1-\Omega_m)}}. \quad (3)$$

However, rather than studying the full 3D, the information contained in the initial few Legendre multipoles or in clustering wedges statistics is utilised. The Legendre multipoles in configuration space

and the power spectrum multipoles are defined respectively as

$$\xi_\ell(s) \equiv \frac{2\ell + 1}{2} \int_{-1}^1 L_\ell(\mu) \xi(\mu, s) d\mu, \quad (4)$$

$$P_\ell(k) \equiv \frac{2\ell + 1}{2} \int_{-1}^1 L_\ell(\mu) P(\mu, k) d\mu, \quad (5)$$

where $\xi(\mu, s)$ and $P(\mu, k)$ are two dimensional correlation function and power spectrum respectively. Here variable μ is the cosine of the angle between the line of sight direction and separation vector s .

The relationship between two-dimensional Legendre multipoles $\xi_\ell(s)$ and $P_\ell(k)$ is described as

$$\xi_\ell(s) \equiv \frac{i^\ell}{2\pi^2} \int_0^\infty P_\ell(k) j_\ell(ks) k^2 dk, \quad (6)$$

j_ℓ here describes the ℓ^{th} order spherical Bessel function. In standard analysis, information just from monopole, quadrupole and hexadecapole ($\ell = 0, 2$ and 4) is used as they have a nearly complete description of the μ dependence of $\xi(\mu, s)$ in distant observer approximation in the linear regime.

Using the power spectrum and two-point correlation function described above, the BAO scale is measured in redshift space. The observable is the shift in the BAO peak position with respect to fiducial cosmology. The parallel and perpendicular shifts to the line of sight give bounds on Hubble expansion rate $H(z)$, comoving and angular diameter distance relative to the sound horizon at drag epoch r_d parameter.

$$\alpha_\perp = \frac{D_M(z) r_{d, fid}}{D_M^{fid}(z) r_d}; \quad \alpha_\parallel = \frac{H^{fid}(z) r_{d, fid}}{H(z) r_d} \quad (7)$$

To illustrate how comoving distance $D_M(z)$ and the Hubble parameter $H(z)$ are measured, consider the preferred angular separation of galaxies, $\Delta\theta$, within an ensemble of galaxy pairs oriented perpendicular to the line of sight. The comoving distance at this redshift is then determined by $D_M(z) = r_d/\Delta\theta$. When examining the separation vector parallel to the line of sight, if a preferred redshift separation Δz is observed, the corresponding equivalent distance is $D_H = c/H(z) = r_d/\Delta z$, thereby inferring the Hubble expansion parameter at that redshift. For certain redshift bins with low signal-to-noise ratios, and when both the transverse and line-of-sight components are present, isotropic BAO (Baryon Acoustic Oscillation) measurements are obtained using $D_V(z)$, where

$$D_V(z) = [(1+z)^2 D_A^2(z) z D_H]^{\frac{1}{3}}. \quad (8)$$

Here, $D_A(z) = D_M(z)/(1+z)$ is the angular diameter distance, and $D_V(z)$ represents the average of the distances measured perpendicular and parallel to the line of sight of the observer (Eisenstein et al. 2005).

The BOSS Survey (Baryon Oscillation Spectroscopic Survey) (Alam et al. 2016) assumes the fiducial cosmology as a flat Λ CDM model with the following parameters: dimensionless Hubble constant $h = 0.676$, fluctuation amplitude $\sigma_8 = 0.8$, baryon density $\Omega_b h^2 = 0.022$, optical depth $\tau = 0.078$ and spectral tilt $n_s = 0.97$. For this model, the sound horizon at the drag epoch parameter is $r_d = 147.78$ Mpc. These parameter values are within 1σ of Planck 2015 values from CMB.

Even when the study was extended beyond Λ CDM models such as ow_0w_a CDM model or $0w$ CDM model with extra relativistic species and by incorporating SN Type I-a dataset, the obtained Hubble Constant value was $H_0 = 67.3 \pm 1.0$ km s⁻¹ Mpc⁻¹ and

$H_0 = 67.8 \pm 1.2$ km s⁻¹ Mpc⁻¹ respectively not shifting from the mean value of standard Λ CDM model ($H_0 = 67.6 \pm 0.5$ km s⁻¹ Mpc⁻¹ (Planck alone)). And, hence keeping the tension with the standard distance ladder SH0ES'22 alive.

2.1.2 Two Point Angular Correlation Function

The two-point angular correlation function (2PACF) is defined as the excess probability of finding two-point sources in two solid angles $d\Omega_1$ and $d\Omega_2$ with angular separation θ as compared to a homogeneous Poisson distribution (Carvalho et al. 2016). To avoid the contribution of radial signal, only narrow redshift shells of very small width δz are considered.

$$\omega(\theta) = \frac{DD(\theta) - 2DR(\theta) + RR(\theta)}{RR(\theta)}, \quad (9)$$

where where $\theta = \theta_{FIT}$ is supposed to be the true bump for the transversal BAO signal. Along with the true BAO signal, many bumps can be observed from 2PACF due to various systematic effects, which can be removed by taking the expected 2PCF. The expected 2PACF can be easily calculated using the expected 2PCF.

$$\omega_E(\theta, \bar{z}) = \int_0^\infty dz_1 \phi(z_1) \int_0^\infty dz_2 \phi(z_2) \xi_E(s, \bar{z}), \quad (10)$$

$$\xi_E(s, z) = \int_0^\infty \frac{dk}{2\pi^2} k^2 j_0(ks) b^2 P_m(k, z), \quad (11)$$

where \bar{z} is the average redshift of z_1 and z_2 , j_0 is the zeroth order Bessel Function and P_m is the matter power spectrum calculated using the fiducial cosmological model Λ CDM with parameters set to $w_b h^2 = 0.0226$, $w_c h^2 = 0.112$, $100\Theta = 1.04$, $\tau = 0.09$, $A_s e^9 = 2.2$, and $n_s = 0.96$ for SDSS DR10 galaxies ((Carvalho et al. 2016)).

Once Θ_{FIT} is estimated, it can be used to infer cosmological distances and therefore put bounds on cosmology. The relation describing the true bump of the BAO signal and angular diameter distance is given by

$$\theta_{BAO} = \frac{r_d}{(1+z)D_A(z)} \quad (12)$$

where $D_A(z)$ is the angular diameter distance and r_d is the sound horizon at the drag epoch.

3 DATA AND METHODOLOGY

In the subsequent sections, we describe the observational datasets utilized in this study.

We commence by detailing the Baryon Acoustic Oscillation (BAO) data, which serves as a basis for comparison. Subsequently, we elucidate the Supernova Type Ia (SN Ia) data, strategically employed to mitigate degeneracies with the BAO measurements. Given the ongoing tension between the Hubble constant (H_0) or the absolute magnitude (M_B) used for calibrating SN Ia, we adopt a comprehensive approach. Rather than relying solely on the M_B derived from local distance ladder measurements, we compile a diverse array of possible M_B values from various probes, facilitating a complete analysis. For the sake of brevity, we designate the theta measurements of BAO, as tabulated in Table 1 simply as "BAO Data - 2D" and data given in Table 2 as "BAO Data - 3D". Furthermore, upon the inclusion of the BAO Dark Energy Spectroscopic Instrument (DESI) dataset, we explicitly refer to it as "BAO Data: DESI", despite its categorization within the BAO

Data-3D framework.

BAO Data - 2D: We employed a dataset comprising 12 Baryon Acoustic Oscillation (BAO) measurements, denoted as $\theta_{\text{BAO}}(z)$, obtained under the assumption of a fiducial cosmology derived from Planck observations. The determination of the BAO angular scale involved conducting a two-point correlation function analysis between pairs of data points. This measurement of the BAO angular scale serves to impose constraints on the absolute scale of BAO, denoted as r_d , once the angular diameter distance (D_A) to the respective redshift is known. The relationship between θ_{BAO} , D_A , and r_d is delineated by Equation (12). Table 1 presents the compiled BAO dataset, encapsulating these measurements for further analysis.

BAO Data - 3D: For the three-dimensional (3D) Baryon Acoustic Oscillations (BAO) data, we amalgamate isotropic BAO measurements obtained from various surveys. These include the 6dF galaxy survey at redshift $z = 0.106$ (Beutler et al. 2011), the SDSS DR7-MGS survey at an effective redshift $z = 0.15$ (Ross et al. 2011), and measurements from the SDSS DR14-eBOSS quasar samples at redshift $z = 1.52$ (Ata et al. 2017). Additionally, BAO measurements using Lyman-alpha samples in conjunction with quasar samples at redshift 2.4 from the SDSS DR12 are incorporated (Bourboux et al. 2017). Furthermore, anisotropic BAO measurements from the BOSS DR12 galaxy sample at redshifts 0.38, 0.51, and 0.61 along with the covariance matrix (Evslin et al. 2018) are utilised. The compiled BAO dataset is presented in Table 2. Henceforth, we collectively refer to these datasets as "3D BAO" data.

SN Type-I: In addition to the Baryon Acoustic Oscillations (BAO) data, we used the expansive "Pantheon Plus Sample" of Type-I Supernovae (SN-Ia), comprising a total of 1701 supernovae spanning the redshift range from 0.01 to 2.26 (Scolnic et al. 2018). This comprehensive dataset incorporates the SH0ES distance anchors, utilizing the host cepheid galaxies for calibration (Table for SN-Ia dataset 2018).

In our analysis, we adopted a range of Hubble Constant values obtained from different techniques. One such instance involves the adoption of a fixed value for the absolute magnitude, $M_B = -19.214 \pm 0.037$ magnitudes. This determination arises from a synthesis of geometric distance estimates derived from Detached Eclipsing Binaries in the Large Magellanic Cloud (LMC) (Pietrzyński et al. 2019), the MASER NGC4258 (Reid et al. 2019), and recent parallax measurements of 75 Milky Way Cepheids with Hubble Space Telescope (HST) photometry (Riess et al. 2021) GAIA Early Data Release 3 (EDR3) (Lindgren et al. 2020a,b). Notably, this represents the most precise and contemporary model-independent assessment of the Absolute Magnitude to date. Other adopted values of M_B used in our analysis are given in Table 3.

Utilizing the Absolute Magnitude of standard candles, such as Type-Ia Supernovae (SNe-Ia), one can readily deduce their distance given their observed apparent magnitude or flux. The relationship between the apparent magnitude of SNe-Ia and their relative distance modulus is expressed by the equation:

$$D_L = 10^{(\mu-25)/5}. \quad (13)$$

Here, $\mu = m_b - M_B$ represents the distance modulus, where m_b denotes the apparent magnitude of SNe-Ia and M_B signifies the absolute magnitude of SNe-Ia.

3.1 Model and Methodology

We aim to compare the constraints on cosmological parameters while using 3D and 2D Baryon Acoustic Oscillations datasets. To keep the analysis as simple as possible and focus on comparing the datasets of BAO, we intentionally assumed a single model of cosmology which is the simplest six-parameter Λ CDM model. We used data combination (BAO + Pantheon Plus) as mentioned in Section 3 to fit the cosmological parameters.

In the Λ CDM cosmology framework, within a spatially flat FLRW universe, the present scale factor a_0 is normalized to 1.0. The Hubble parameter at redshift z is given by:

$$\frac{H^2(z)}{H_0^2} = \Omega_{m0}(1+z)^3 + (1-\Omega_{m0}), \quad (14)$$

where the subscript 0 denotes present-day values and Ω_{m0} represents the present-day matter density. Other relevant quantities are defined as follows:

$$D_M(z) = \int_0^z \frac{c d\bar{z}}{H(\bar{z})}, \quad (15)$$

$$D_A(z) = (1+z)^{-1} D_M(z), \quad (16)$$

$$D_L(z) = (1+z) D_M(z), \quad (17)$$

$$D_V(z) = ((1+z) D_A(z))^{2/3} \left(\frac{cz}{H(z)} \right)^{1/3} \quad (18)$$

where D_M , D_A and D_L are comoving distance, angular diameter distance and luminosity distance respectively.

We applied a uniform prior distribution on Ω_{m0} , h , and r_d as outlined in Table 3. Rather than relying solely on a single calibration for the absolute magnitude M_B of the SN sample, we opted to consider multiple values of M_B (or equivalently, H_0), a practice also observed in various studies such as Lemos et al. (2023). For conversion, we employed the relation:

$$M_B = 5(\log H_0 - \alpha_B - 5), \quad (19)$$

where α_B is the observed intercept of B band apparent magnitude-redshift relation for SNe in the Hubble flow. Presently, we assumed its value to be 0.71273 ± 0.00176 obtained independently of CMB and BAO. We employed Gaussian priors on M_B derived from various measurements of the Hubble Constant, including those from ACT+WMAP CMB, Planck CMB + Lensing, SH0ES collaborations, values derived from Masers, the Tully Fisher Relation, and BOSS DR12+BBN, as detailed in Table 3. For generating Markov Chain Monte Carlo (MCMC) chains based on the aforementioned dataset, we utilized the publicly available code EMCEE (Foreman-Mackey et al. 2013). The obtained results are presented in Table 4.

3.2 Cosmological Chisq Analysis

To infer information about the cosmological parameters within the framework of the flat Λ CDM model, we conducted a Chisq analysis utilizing the observables from the BAO 3D and BAO 2D datasets.

For the BAO 2D data, the observable is $\theta_{\text{BAO}}(z)$ as defined in Equation (12). The corresponding chi-squared function is given by:

$$\chi_{2D \text{ BAO}}^2(H_0, \Omega_{m0}, r_d) = \sum_i \left[\frac{\theta_{\text{BAO}}(z_i)^{\text{obs}} - \theta_{\text{BAO}}(z_i)^{\text{model}}}{\sigma_{\theta_{\text{BAO}}(z_i)}} \right]^2, \quad (20)$$

Table 1. BAO measurements from angular separation of pairs of galaxies (denoted as BAO Dataset: 2D throughout the analysis).

\bar{z}	$\theta_{\text{BAO}}(z)[^\circ]$	Reference	\bar{z}	$\theta_{\text{BAO}}(z)[^\circ]$	Reference
0.45	4.77 ± 0.17	SDSS DR10 [(Carvalho et al. 2016)]	0.57	4.59 ± 0.36	SDSS DR11 [(Carvalho et al. 2017)]
0.47	5.02 ± 0.25	SDSS DR10 [(Carvalho et al. 2016)]	0.59	4.39 ± 0.33	SDSS DR11 [(Carvalho et al. 2017)]
0.49	4.99 ± 0.21	SDSS DR10 [(Carvalho et al. 2016)]	0.61	3.85 ± 0.31	SDSS DR11 [(Carvalho et al. 2017)]
0.51	4.81 ± 0.17	SDSS DR10 [(Carvalho et al. 2016)]	0.63	3.90 ± 0.43	SDSS DR11 [(Carvalho et al. 2017)]
0.53	4.29 ± 0.30	SDSS DR10 [(Carvalho et al. 2016)]	0.65	3.55 ± 0.16	SDSS DR11 [(Carvalho et al. 2017)]
0.55	4.25 ± 0.25	SDSS DR10 [(Carvalho et al. 2016)]	2.225	1.77 ± 0.31	SDSS QS [(de Carvalho et al. 2018)]

Table 2. BAO measurements from volumetric measurements (denoted as BAO Dataset: 3D throughout the analysis).

z	Anisotropic Constraint	Reference	z	Isotropic Constraint	Reference
0.38	$\frac{D_A(0.38)}{r_d} = 7.42$	BOSS DR 12 [(Alam et al. 2017)]	0.106	$\frac{D_V(0.106)}{r_d} = 2.98 \pm 0.13$	6dF [(F. Beutler et al 2011)]
0.38	$\frac{D_H(0.38)}{r_d} = 24.97$	BOSS DR 12 [(Alam et al. 2017)]	0.15	$\frac{D_V(0.15)}{r_d} = 4.47 \pm 0.17$	MGS [(Ross et al. 2015)]
0.51	$\frac{D_A(0.51)}{r_d} = 8.85$	BOSS DR 12 [(Alam et al. 2017)]	1.52	$\frac{D_V(1.52)}{r_d} = 26.1 \pm 1.1$	eBOSS quasars [(Ata et al. 2017)]
0.51	$\frac{D_H(0.51)}{r_d} = 22.31$	BOSS DR 12 [(Alam et al. 2017)]			
0.61	$\frac{D_A(0.61)}{r_d} = 9.69$	BOSS DR 12 [(Alam et al. 2017)]			
0.61	$\frac{D_H(0.61)}{r_d} = 20.49$	BOSS DR 12 [(Alam et al. 2017)]			
2.4	$\frac{D_A(2.4)}{r_d} = 10.76$	BOSS DR 12 [(Bourboux et al. 2017)]			
2.4	$\frac{D_H(2.4)}{r_d} = 8.94$	BOSS DR 12 [(Bourboux et al. 2017)]			

For the BAO 3D data, we have both anisotropic and isotropic observables. Equation (21) describes the anisotropic component, where D_i represents the best fit of observables as $D_A(z_i)/r_d$ and $D_M(z_i)/r_d$ respectively. The covariance matrix for this dataset can be found in Table 1 of (Evslin et al. 2018).

$$\chi_{\text{3D BAO}}^2 = \sum_{i,j} [D_i^{\text{obs}} - D(z_i)^{\text{model}}] \text{Cov}_{i,j}^{-1} [D_j^{\text{obs}} - D(z_j)^{\text{model}}], \quad (21)$$

Further, for the isotropic component of the BAO 3D data, the observable is $D_V(z_i)/r_d$, where $D_V(z_i)$ is the volume-averaged distance. The Chi-squared definition for this component is provided below in Equation (22):

$$\chi_{\text{3D BAO}}^2 = \sum_i \left[\frac{D_V(z_i)/r_d^{\text{obs}} - D_V(z_i)/r_d^{\text{model}}}{\sigma_{(D_V(z_i)/r_d)}} \right]^2, \quad (22)$$

For minimising the supernova cosmology parameters, the χ^2 function is defined as in Equation (23), where μ_i represents each supernova distance, with i ranging from 1 to 1701. $\mu_{b,i}^{\text{model}}$ denotes the predicted distance modulus, estimated using cosmological parameters describing the expansion history (here, Λ CDM).

$$\chi_{\text{SNe-Ia}}^2(H_0, \Omega_{m0}, M_B) = \sum_{i,j} [\mu_{b,i}^{\text{obs}} - \mu_{b,i}^{\text{model}}] \text{Cov}_{i,j}^{-1} [\mu_{b,j}^{\text{obs}} - \mu_{b,j}^{\text{model}}], \quad (23)$$

And, $\text{Cov}_{i,j}^{-1}$ describes the covariance matrix for supernova data. The total chi-square is then defined as the sum of the chi-square contributions from the Pantheon Plus sample and the BAO sample, where "BAO" encompasses both BAO datasets used for comparison.

$$\chi_{\text{Total}}^2(H_0, \Omega_{m0}, M_B, r_d) = \chi_{\text{SNe-Ia}}^2(H_0, \Omega_{m0}, M_B) + \chi_{\text{BAO}}^2(H_0, \Omega_{m0}, r_d). \quad (24)$$

4 RESULTS AND DISCUSSION

4.1 Tension between BAO 3D Data and BAO 2D Data

4.1.1 Effect on the sound horizon at the drag epoch: The Standard Ruler

In this section, we present the results of our analysis and discuss the tension observed between the two BAO datasets: 3D and 2D. Specifically, we focus on the cosmological parameter r_d , which represents the sound horizon at the drag epoch. Previous studies have confirmed a high correlation between H_0 and r_d . For instance, from Planck observations, the derived H_0 is $67.27 \pm 0.60 \text{ km s}^{-1} \text{ Mpc}^{-1}$, corresponding to r_d of $147.05 \pm 0.30 \text{ Mpc}$. However, other studies such as (Evslin et al. 2018) have found that when H_0 is constrained from low-redshift studies, its value tends to be around $\sim 73 \text{ km s}^{-1} \text{ Mpc}^{-1}$, requiring r_d to be $\sim 137 \text{ Mpc}$, leading to a tension of more than 2.5 sigmas with Planck, regardless of the behaviour of dark energy.

It is crucial to note that this discrepancy arises when using the 3D BAO data. We got similar results as one can see in Table 4. While using 3D BAO data and Pantheon Plus with SH0ES 2021_a calibration, we got constraints on r_d as $134.30 \pm 2.41 \text{ Mpc}$ corresponding to h constraints 0.75 ± 0.012 . Conversely, when utilizing the 2D BAO data, we obtained h as 0.745 ± 0.0129 , corresponding to r_d of $142.22 \pm 3.37 \text{ Mpc}$, which is compatible with the Planck value of r_d within one sigma (see Figure 2).

We have extensively examined this dataset to further understand the cosmological tensions and the impact of the BAO dataset. To facilitate a comprehensive discussion, we have divided our analysis into two subsections:

a) Pantheon Plus Calibration with M_B Compatible with Low-Redshift Experiments

Our analysis involved utilizing five different measurements of H_0 from various low-redshift studies. We estimated the absolute magnitude of Type-Ia Supernovae (M_B) from these measurements to calibrate our Pantheon Plus sample. As illustrated in Table 4, the upper-left portion, utilizing the Pantheon Plus and BAO Data: 3D,

Parameter	Prior
Ω_{m0}	[0.1, 0.9]
h	[0.50, 0.90]
r_d	[130, 170]
Measurements of M_B	Prior (Gaussian($\mathcal{N}(\mu, \sigma^2)$))
Planck CMB + Lensing	$\mathcal{N}(-19.422, 0.019^2)$
ACT + WMAP CMB	$\mathcal{N}(-19.414, 0.036^2)$
BOSS DR12 + BBN	$\mathcal{N}(-19.385, 0.070^2)$
SHOES 2021 _a	$\mathcal{N}(-19.214, 0.039^2)$
SHOES 2021	$\mathcal{N}(-19.241, 0.040^2)$
Masers	$\mathcal{N}(-19.220, 0.089^2)$
SHOES 2019	$\mathcal{N}(-19.217, 0.042^2)$
Tully Fisher	$\mathcal{N}(-19.159, 0.075^2)$

Table 3. Parameters used and their prior.

yielded an estimated $r_d \sim 135$ Mpc, exhibiting more than three sigma tension with Planck’s estimation of r_d . Conversely, when employing the 2D BAO Data alongside the same Pantheon Plus sample and the same calibration of M_B , we obtained r_d elevated to around 142 Mpc, aligning with Planck’s r_d within one sigma (see Figure 2).

From this analysis, we infer that while the tension in H_0 between Planck and SHOES is confirmed, there is no tension in r_d when using the 2D data. With H_0 around $73 \text{ km s}^{-1} \text{ Mpc}^{-1}$, we achieve an r_d of roughly 142 Mpc, compatible with Planck. To ensure the robustness of our results independent of the calibration of the Pantheon Plus sample, we consider calibrations of M_B from various experiments. Notably, our findings from all low-redshift experiments converge, indicating mutual consistency.

b) Pantheon Plus Calibration with M_B Compatible with High-Redshift Experiments

We calibrated the Pantheon Plus sample using M_B calibration from three H_0 measurements for high redshifts, namely Planck CMB + Lensing, BOSS DR12 + BBN, and ACT+WMAP CMB. We found that with the Pantheon Plus calibrated to high-redshift experiments, we obtained h value around 0.67 and r_d close to 147 Mpc while using the BAO 3D data. However, when utilizing the BAO 2D data with the same calibration, we obtained the same H_0 value but r_d as 156 Mpc, which exhibits tension with Planck’s value of r_d .

In the previous subsections, we talked about r_d tension between 2D and 3D BAO, and we found our results depend a lot on which SNe calibration M_B we used. We need to understand here, that since 2D BAO measures a higher product of hr_d than 3D BAO (Equation 26 and 25), a higher rd corresponding to higher h can be allowed. For example, while using 2D BAO and SHOES 2021_a calibration, h of 0.745 ± 0.0129 is allowed corresponding to r_d 142.22 Mpc. On the other hand, in 3D BAO and SHOES 2021_a calibration, h of 0.75 ± 0.012 allows lower value r_d 134.30 ± 2.41 Mpc. From here we conclude that from BAO data, we should not conclude on h and r_d individually but the product $r_d h$.

4.1.2 Cosmological constraints on the product $r_d * h$

Figure 4 confirms that the result we obtained is completely in alignment with the fact that the product of Hubble Constant and BAO acoustic scale $H_0 r_d$ is constant irrespective of calibration of SNe Ia used. We can also say that it is the artefact of the fact that BAO measurements put bounds on $H(z)r_d$ rather than individually putting constraints on r_d or H_0 (Bernel et al. 2016). Also in CMB measurements, we measure the angular acoustic scale $r_d/D_A(z_d)$ where z_d

is the drag epoch redshift. In Figure 4, all the $H_0 r_d$ values while using BAO Data: 3D agree within one sigma irrespective of the M_B (SNe calibration) used. The same is true for the BAO 2D Dataset. We also plotted green and orange bands using CMB temperature, polarization, and lensing. ($r_d h = 101.8 \pm 1.3 \text{ Mpc}$) and from DESI which is $r_d h = 98.82 \pm 0.82 \text{ Mpc}$. The mean value of $H_0 r_d$ from PP + 3D BAO data coincides with the CMB band except for the cases when Pantheon Plus utilises Tully Fisher or Masers for calibrating the sample. DESI Band does not overlap with the CMB band within one sigma. But within two sigmas, products from both BAO datasets 2D and 3D are consistent (Equation 25 and Equation 26). DESI BAO uses the same methodology as our denoted BAO: 3D dataset. BAO 2D dataset also shows tension with CMB obtained $H_0 r_d$ results. We obtained the following results assuming SHOES_a calibration for Pantheon Plus along with BAO datasets. We mentioned the BAO dataset we used and the results stated are in 68 % credible interval.

$$\left. \begin{aligned} \Omega_{m0} &= 0.314 \pm 0.0132 \\ r_d h &= 100.72 \pm 2.42 \text{ Mpc} \end{aligned} \right\} \text{BAO : 3D + PP} \quad (25)$$

$$\left. \begin{aligned} \Omega_{m0} &= 0.331 \pm 0.018 \\ r_d h &= 105.95 \pm 3.11 \text{ Mpc} \end{aligned} \right\} \text{BAO : 2D + PP} \quad (26)$$

5 COMMENTS ON COSMOLOGICAL MODEL USED

While keeping in mind that BAO measures the product of $H_0 r_d$ and not H_0 and r_d individually, the presented results (Figure 2-left plot) and the last subsection reveal around 1.3σ tension within two independent BAO datasets: 2D BAO and 3D BAO datasets and less than two sigmas tension between CMB and DESI estimated $H_0 r_d$. But if we look at contour $H_0 r_d - \Omega_{m0}$ (Figure 2-right plot), the tension in $H_0 r_d - \Omega_{m0}$ contours is more than two sigma. We can clearly see that there is no tension between Ω_{m0} of 2D BAO, 3D BAO and CMB estimated Ω_{m0} . This tension in $H_0 r_d$ from 2D and 3D BAO appeared because of $\Omega_{m0} - H_0 r_d$ correlation. Now this tension in $H_0 r_d$ from 2D and 3D BAO in $\Omega_{m0} - H_0 r_d$ plane calls for questioning the relation between Ω_{m0} and $H_0 r_d$ which comes from assuming a cosmological model. Here the assumed cosmological model is Λ CDM. As can be seen from Figure 2 (left plot), there is no tension (around 1σ) between 2D and 3D BAO datasets, Λ CDM is in trouble (beyond 2σ) assuming there is no systematic error in BAO.

6 ANALYSIS WITH DESI DATA

6.1 Model, Methodology, and Dataset

In our analysis with DESI data, we adhered to the standard cosmological model, Λ CDM, to compare with the results obtained in the previous sections. However, to highlight DESI’s main findings, we extended our analysis to include the Chevallier-Polarski-Linder (CPL) model, which introduces a redshift-dependent equation of state parameter $w(z) = w_0 + w_a(1 - a) = w_0 + w_a \frac{z}{1+z}$, providing a more nuanced characterization of cosmic dynamics.

In the CPL model, the Hubble parameter $H(z)$ is expressed as:

$$\frac{H^2(z)}{H_0^2} = \Omega_{m0}(1+z)^3 + (1 - \Omega_{m0})f(z), \quad (27)$$

where $f(z) = \exp\left(3 \int^z \frac{(1+w(x))}{1+x} dx\right)$.

Measurements	Panth Plus + BAO Data : 3D			Panth Plus + BAO Data : 2D		
	r_d (Mpc)	h	Ω_{m0}	r_d (Mpc)	h	Ω_{m0}
SH0ES 2021 _a	134.30 ± 2.41	0.75 ± 0.012	0.314 ± 0.0132	142.22 ± 3.37	0.745 ± 0.0129	0.331 ± 0.0179
SH0ES 2021	135.78 ± 2.73	0.74 ± 0.01	0.315 ± 0.0133	143.93 ± 3.56	0.736 ± 0.013	0.3315 ± 0.0181
Masers	136.53 ± 4.46	0.73 ± 0.02	0.314 ± 0.0133	143.026 ± 6.22	0.742 ± 0.029	0.3306 ± 0.0178
SH0ES 2019	134.58 ± 2.67	0.74 ± 0.01	0.314 ± 0.0133	142.359 ± 3.622	0.744 ± 0.014	0.3308 ± 0.018
Tully Fisher	134.05 ± 3.04	0.75 ± 0.02	0.313 ± 0.0132	139.05 ± 4.91	0.762 ± 0.024	0.331 ± 0.0179
Planck CMB + Lensing	147.44 ± 1.89	0.67 ± 0.01	0.315 ± 0.0134	156.36 ± 2.90	0.677 ± 0.006	0.330 ± 0.0178
BOSS DR12 + BBN	145.02 ± 4.82	0.69 ± 0.022	0.314 ± 0.0135	153.92 ± 5.55	0.688 ± 0.022	0.331 ± 0.0182
ACT + WMAP CMB	146.89 ± 2.84	0.68 ± 0.01	0.315 ± 0.0133	155.86 ± 3.64	0.679 ± 0.011	0.3312 ± 0.0179

Table 4. Constraints on parameters for Λ CDM for both BAO Data Sets and various Pantheon Plus calibrations M_B . The error bars quoted are at 1σ confidence interval.

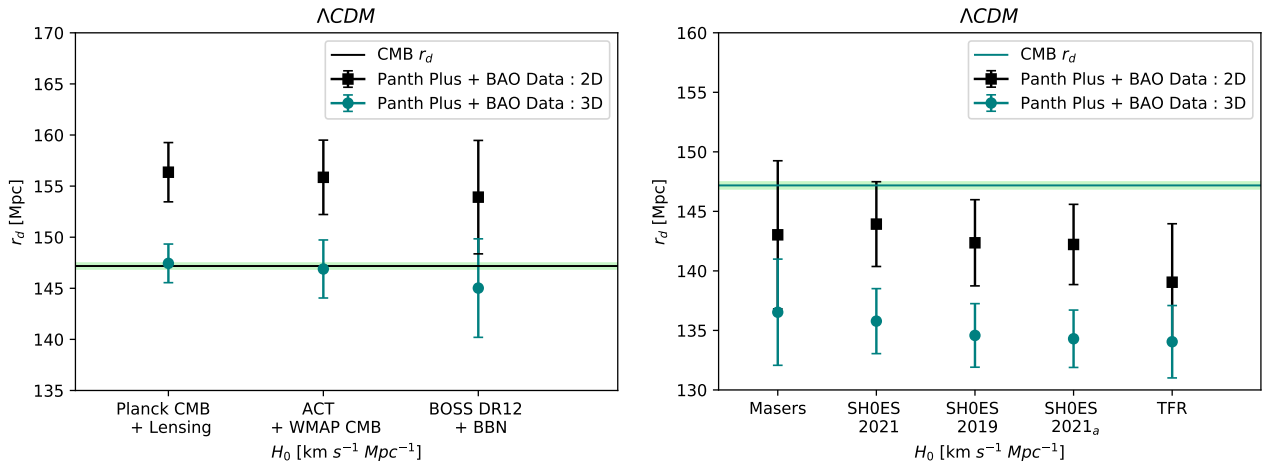


Figure 1. This plot shows different H_0 values obtained from various measurements - high (left) and low redshifts (right) on the x-axis. On the Y axis are the constraints on the r_d (absolute scale of Baryon Acoustic Oscillations). The green band in both plots shows constraints on r_d from the CMB Planck experiment.

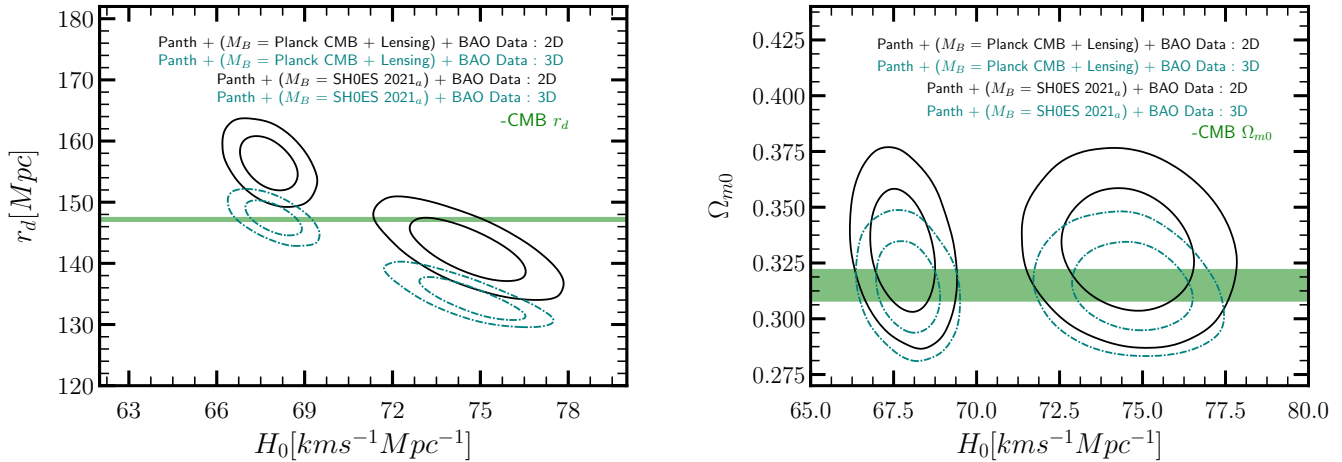


Figure 2. This plot shows $H_0 - r_d$ contours and the correlation of H_0 and r_d while using two different BAO Datasets and two different calibrations M_B for Pantheon Plus sample. The horizontal green band represents CMB Planck r_d .

Other than the Pantheon Plus dataset and DESI BAO dataset as provided in Table 5, we also incorporated CMB data. In particular, we utilised the *Planck* 2018 compressed likelihood for TT, TE, EE + lowE as obtained by Chen et al. (?) (for the detailed method for

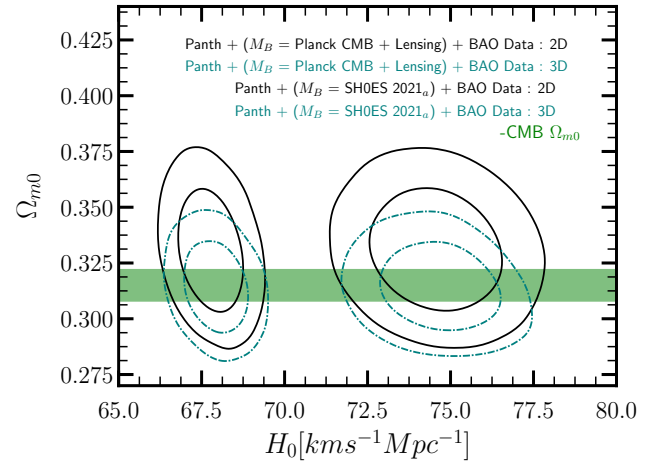


Figure 3. This plot shows $H_0 - \Omega_{m0}$ contours and the correlation of H_0 and Ω_{m0} while using two different BAO Datasets and two different calibrations M_B for Pantheon Plus sample. The horizontal green band represents CMB Planck Ω_{m0} .

obtaining the compressed likelihood (see Ade et al. (?)). We applied the same methodology and definitions used for conducting the Chisq analysis of the 3D BAO dataset to analyze the DESI data. This includes the Equation (21) and Equation (22) used for calcu-

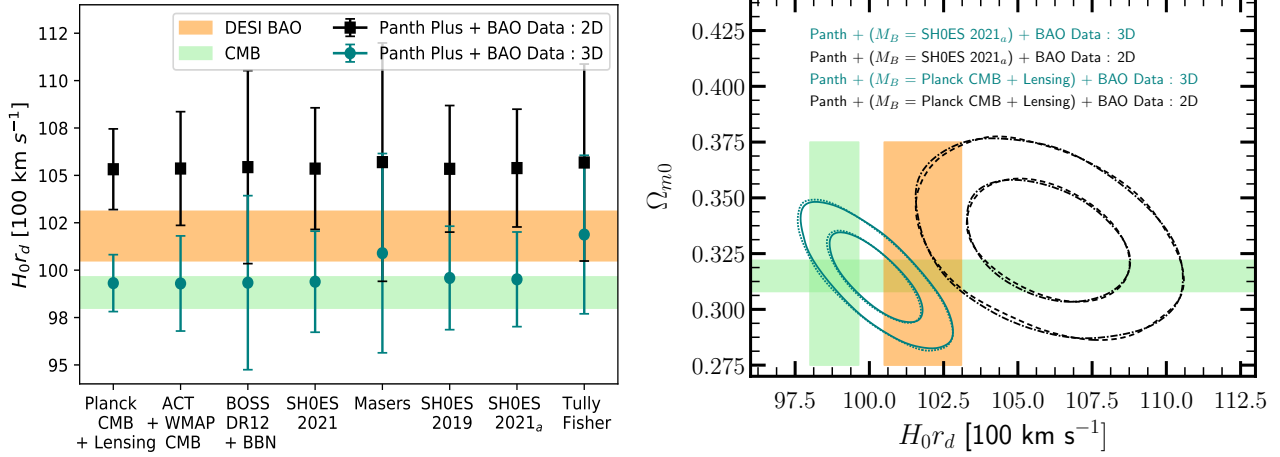


Figure 4. Left: This plot shows the values of the product of the Hubble parameter and sound horizon at the drag epoch $r_d h$ obtained while utilising various calibrations for the Pantheon Plus sample and two different BAO datasets. Right: This plot shows the contours of $r_d h$ and Ω_{m0} matter density at present obtained for various calibrations for the Pantheon Plus sample when combined with two different BAO datasets. The orange and light green bands used for comparison are the results from DESI ($r_d h = 101.8 \pm 1.3$ Mpc) and CMB temperature, polarization and lensing ($r_d h = 98.82 \pm 0.82$ Mpc and $\Omega_{m0} = 0.315 \pm 0.007$) respectively. We used the notation $r_d h \equiv H_0 r_d / (100 \text{ km s}^{-1} \text{ Mpc}^{-1})$ in both plots.

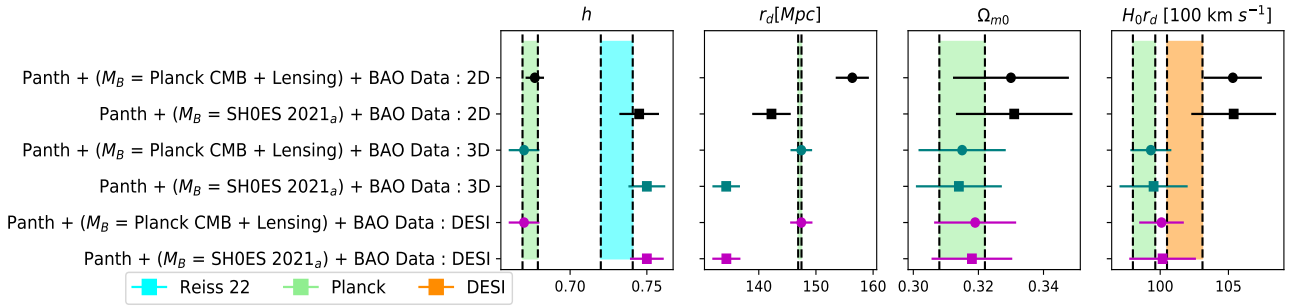


Figure 5. This plot shows three cosmological parameters h , r_d , Ω_{m0} along with the product of Hubble parameter and sound horizon at the drag epoch $H_0 r_d$ obtained using various calibration for Pantheon Plus sample combined with two different BAO datasets. In the h subplot, we show green and cyan bands from Planck 2018 and Reiss '22 for comparison. In the r_d and Ω_{m0} subplots, we show Planck corresponding values. Further in the extreme right subplot of $H_0 r_d$, the orange and light green bands used for comparison are the results from DESI ($r_d h = 101.8 \pm 1.3$ Mpc) and CMB temperature, polarization and lensing ($r_d h = 98.82 \pm 0.82$ Mpc). We used the notation $r_d h \equiv H_0 r_d / (100 \text{ km s}^{-1} \text{ Mpc}^{-1})$.

Tracer	z	DM/rd	DH/rd	DV/rd
BGS	0.30	-	-	7.93 ± 0.15
LRG	0.51	13.62 ± 0.25	20.98 ± 0.61	-
LRG	0.71	16.85 ± 0.32	20.08 ± 0.60	-
LRG+ELG	0.93	21.71 ± 0.28	17.88 ± 0.35	-
ELG	1.32	27.79 ± 0.69	13.82 ± 0.42	-
QSO	1.49	-	-	26.07 ± 0.67
Lya QSO	2.33	39.71 ± 0.94	8.52 ± 0.17	-

Table 5. DESI Data Release 1 BAO Measurement used

lating the Chisq values for the DESI dataset. The results obtained for the Λ CDM model are presented in Table 6. Our study involved a comparison of data while maintaining the same model. Table 4, Table 6, and Figure 5 depict the comparison of three BAO datasets and their impact on cosmological parameters under the assumption of cosmology as standard Λ CDM. Additionally, Figure 6 and Figure 7 illustrate this comparison using the CPL model.

7 DISCUSSION OF 3D, 2D AND DESI BAO RESULTS

Here, we delve into the results and comparison between the 3D and 2D BAO datasets, alongside the new DESI data release. Figure 5 shows the comparison of three cosmological parameters h , r_d , Ω_{m0} along with the product of Hubble parameter and sound horizon at the drag epoch $H_0 r_d$ obtained while using various calibrations for Pantheon Plus sample and combined with three BAO datasets 2D, 3D and BAO. In the h subplot, we show green and cyan bands from Planck 2018 and Reiss '22 for comparison. In the r_d and Ω_{m0} subplots, we show Planck corresponding values. Further in the extreme right subplot of $H_0 r_d$, the orange and light green bands used for comparison are the results from DESI ($r_d h = 101.8 \pm 1.3$ Mpc) and CMB temperature, polarization and lensing ($r_d h = 98.82 \pm 0.82$ Mpc). We used the notation $r_d h \equiv H_0 r_d / (100 \text{ km s}^{-1} \text{ Mpc}^{-1})$. And, since to distinguish among BAO and conclude irrespective of Pantheon calibration, one should focus on the quantity which BAO measures, the product of $h r_d$. As we can see here, within 2σ both 2D and 3D BAO agree with DESI and CMB obtained $h r_d$.

In Figure 6, we present the $w_0 - w_a$ and $h - r_d$ planes. Both plots

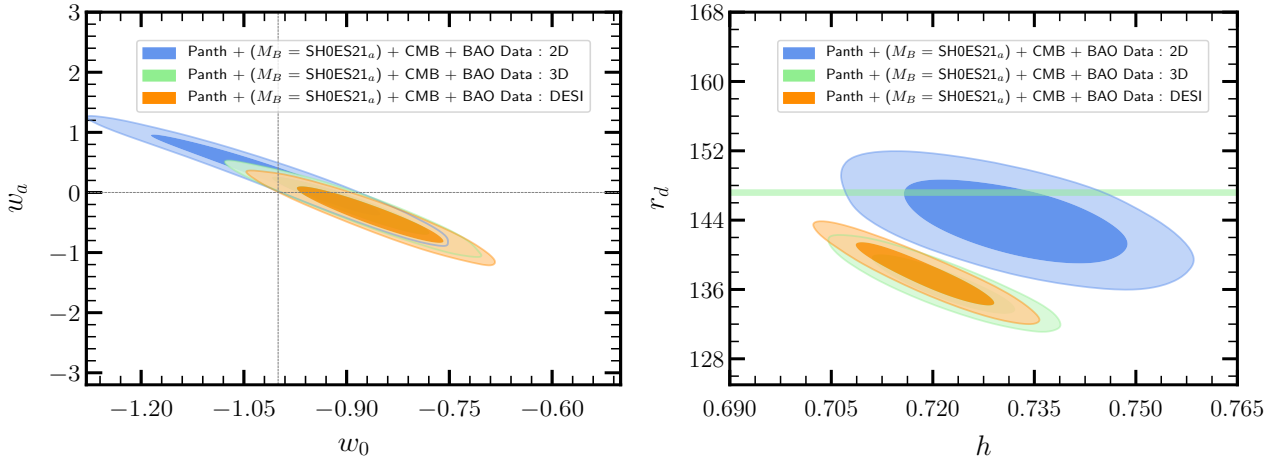


Figure 6. Left : This plot shows how the $w_0 - w_a$ contour plot shifts when we replace 3D dataset to 2D dataset. It also shows that the BAO 3D and DESI BAO datasets have contours that are nearly overlapping. Right: This plot shows three $h - r_d$ contours for the combination of Pantheon Plus + CMB + BAO dataset. It clearly agrees with the fact that the product hr_d for BAO : 2D is greater than that for BAO : 3D or BAO DESI. Keeping h constant, r_d estimated values from Panth Plus + BAO : 2D data combination agrees with Planck r_d within one sigma while Planck r_d is more than 2σ away from Panth Plus + BAO 3D estimate. In both the plots, it is evident that BAO 3D has less constraining power hence giving bigger contours than the BAO 3D dataset.

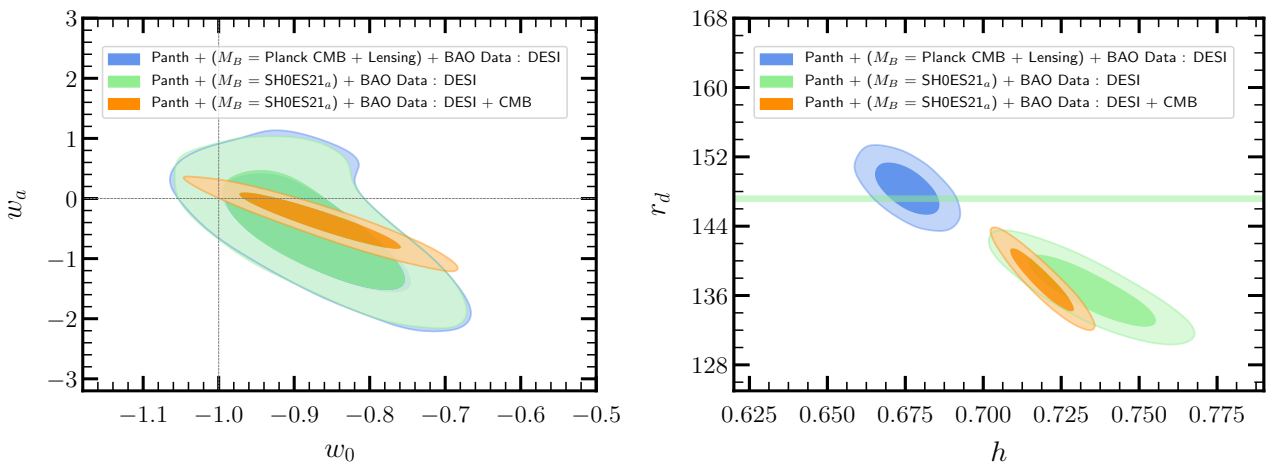


Figure 7. Both the plots have BAO DESI datasets. These plots show how the results change when changing calibration M_B of the Pantheon Plus sample. Left: This plot shows that there is no change in the $w_0 - w_a$ plane when we change the calibration of Pantheon Plus. It also shows how the constraints get better as we add CMB data. Right: We can see the shrink in the $h - r_d$ contours when we added the CMB data set to the Panth Plus + BAO : DESI dataset. We can also see the parallel shift in both the parameters which is a decrease in h and an increase in r_d while we changed the calibration on the Pantheon Plus sample from SH0ES21_a to Planck CMB + Lensing. When data combination Panth + ($M_B = \text{SH0ES21}_a$) + BAO : DESI + CMB is used, the estimated h value is higher because of chosen M_B calibration and estimated h values are between SHOES and CMB and preferring lower r_d than Planck. However, when CMB data is removed and calibration of Pantheon Plus is changed to Planck CMB + Lensing, the lower h is preferred and r_d is then pushed to a higher value keeping the product hr_d constant.

feature the Pantheon Plus sample calibrated with SH0ES21_a along with CMB data, and three BAO datasets: 2D, 3D, and DESI Release.

In the left contour plot, showcasing the $w_0 - w_a$ plane, it's notable that the $(-1.0, 0)$ point lies on the edge of the two-sigma contour across all three datasets. The DESI and 3D BAO datasets exhibit comparable constraining power, while the 2D dataset displays larger contours. Moreover, the contour in the one-sigma region extends towards lower values of w_0 and higher values of w_a for the 2D dataset, while maintaining the correlation. In the right plot, a particularly noteworthy observation emerges. By maintaining consistency

with the other two datasets and solely altering the BAO datasets, a significant finding surfaces: when utilizing the BAO 2D dataset, our estimated r_d aligns with Planck's r_d within a one-sigma region. However, for the other two datasets, 3D and DESI Release, the constraints on r_d deviate from Planck's r_d by more than two sigma.

In Figure 7, the orange contour is the same as in Figure 6 and is provided for comparison and reference. In the left plot, we observe that the contours expand notably when the CMB dataset is removed. Interestingly, altering the calibration of the Pantheon Plus sample does not induce significant changes in the behaviour of the $w_0 - w_a$

Panth Plus + BAO Data : DESI			
Measurements	r_d (Mpc)	h	Ω_{m0}
SHOES 2021 _a	134.33 ± 2.46	0.75 ± 0.011	0.318 ± 0.0124
SHOES 2021	135.83 ± 2.74	0.74 ± 0.013	0.318 ± 0.0125
Masers	136.56 ± 4.44	0.73 ± 0.02	0.317 ± 0.0126
SHOES 2019	134.68 ± 2.67	0.74 ± 0.01	0.318 ± 0.0123
Tully Fisher	134.26 ± 3.12	0.75 ± 0.02	0.311 ± 0.0120
Planck CMB + Lensing	147.44 ± 1.95	0.68 ± 0.01	0.319 ± 0.0126
BOSS DR12 + BBN	145.10 ± 4.87	0.69 ± 0.022	0.318 ± 0.0127
ACT + WMAP CMB	146.95 ± 2.82	0.68 ± 0.01	0.318 ± 0.0127

Table 6. Constraints on parameters for Λ CDM for BAO Data DESI data. The error bars quoted are at 1σ confidence interval.

contours. However, it does lead to substantial shifts in the values of both parameters h and r_d in the right plot.

This outcome was obtained while employing the CPL parameterization and utilizing the DESI dataset. It's worth highlighting that similar results were obtained for the Λ CDM model and the BAO: 3D dataset, as outlined in Table 4. This consistency across different models underscores the robustness and reliability of the findings, indicating that our results are independent of dark energy behaviour.

This finding underscores the unique power of the BAO dataset in providing cosmological constraints that closely align with Planck's measurements. Such alignment underscores the dataset's robustness and its potential to enhance our understanding of the universe's fundamental parameters and break residual degeneracies with CMB. Observations from BAO 2D and BAO 3D provide a promising avenue for resolving discrepancies and refining our understanding of cosmological parameters. Understanding $\Omega_{m0} - H_0 r_d$ plane (in Figure 4) and decreasing tension between the contours while using the 2D and 3D BAO dataset, may require physics beyond Λ CDM not just while inferring cosmological information from cosmological data but also in the assumption of fiducial cosmology in observational data such as parameter α (Equation 7).

8 CONCLUSIONS

Through a critical examination and detailed analysis of 2D and 3D data of BAO and using the theoretical framework of the standard model of cosmology, we aim to check consistency in two BAO datasets. Through careful analysis, we found out that the product of hr_d in both 2D and 3D BAO datasets is consistent. However, more than two sigma tension in $\Omega_{m0} - H_0 r_d$ plane while using two independent BAO datasets may advocate for the need for beyond Λ CDM physics not just while inferring cosmological information from observational data but also while observing BAO datasets and injecting standard assumptions not too different from Λ CDM.

ACKNOWLEDGEMENTS

The author Ruchika would like to thank Alessandro Melchiorri, M. M. Skeikh Jabbari, Nils Schöneberg, Jalison Alcaniz, Thais Lemos and Anjan Ananda Sen for useful discussions. We acknowledge IUCAA, Pune, India for the use of their computational facilities. We acknowledge financial support from TASP, iniziativa specifica INFN.

APPENDIX A: BAO DATA FOR REDSHIFT LESS THAN 1

To assess the potential bias introduced by BAO data at redshifts greater than one, we removed BAO data for redshift $z > 1$ and

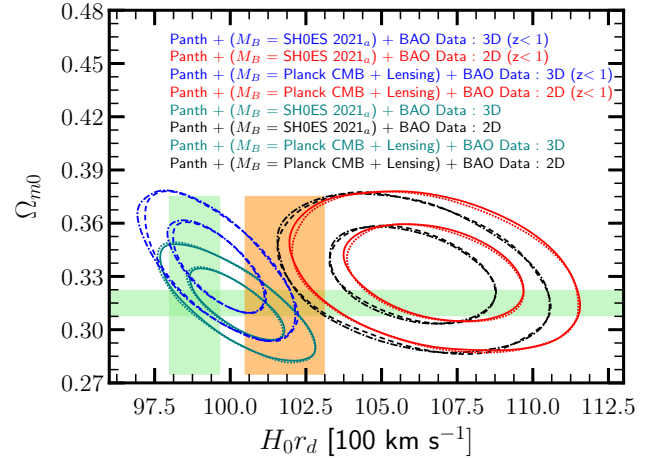


Figure A1. This plot shows the contours of $r_d h$ and Ω_{m0} matter density at present obtained for various calibrations for the Pantheon Plus sample when combined with two different BAO datasets (Teal and Black contours are for full BAO dataset whereas blue and red contours are for BAO Dataset ($z < 1$)). The orange and light green bands used for comparison are the results from DESI ($r_d h = 101.8 \pm 1.3$ Mpc) and CMB temperature, polarization and lensing ($r_d h = 98.82 \pm 0.82$ Mpc and $\Omega_{m0} = 0.315 \pm 0.007$) respectively. We used the notation $r_d h \equiv H_0 r_d / (100 \text{ km s}^{-1} \text{ Mpc}^{-1})$ in the plot.

performed the analysis again. The results are similar to those obtained when all BAO redshift measurements were included (Figure A1). However, the contours obtained while using 3D BAO data shift toward a higher value of Ω_{m0} . Despite this shift, our conclusion that there is more than two-sigma tension in $H_0 r_d$ in $\Omega_{m0} - H_0 r_d$ plane remains unchanged.

References

- Ade P. A. R. et al., 2016a, *Astron. Astrophys.*, **594**, A13
- Ade P. A. R. et al., 2016b, *Astron. Astrophys.*, **594**, A14
- Aghanim N., et al., 2018; 1807.06209.
- Aghanim, N. et al. *Astron. Astrophys.* 2020, 641, A6.
- Aiola S. et al. (ACT), 2020, *JCAP*, 12, 047, arXiv:2007.07288.
- Alam S. et al. *Mon. Not. Roy. Astron. Soc.* 470 (2017) no.3, 2617
- Alam S. et al. (BOSS), *Mon. Not. Roy. Astron. Soc.* 470, 2617 (2017),
- Alam S. et al. *Mon. Not. Roy. Astron. Soc.* 470 (2017) 3, 2617-2652
- Alam S. et al. *MNRAS*, Volume 470, Issue 3, arXiv:1607.03155
- Alam S. et al. (BOSS), *Mon. Not. Roy. Astron. Soc.* 470, 2617 (2011)
- Anselmi S. et al. *Phys. Rev. D* 107, 123506
- Ata M. et al., *Mon. Not. Roy. Astron. Soc.* 473, 4773 (2017)
- Bernal J. L. et al, *JCAP*10(2016)019.
- Betoule M. et al., 2014, [SDSS Collaboration], *Astron. Astrophys.* **568**, A22

Beutler et al. *Mon. Not. Roy. Astron. Soc.* 416, 3017 (2011)
 Beutler F. et al., *Mon. Not. Roy. Astron. Soc.* 416, 3017 (2011)
 Beutler F. et al., 2011, *Mon.Not.Roy.Astron.Soc.*, **416**, 3017
 Beutler F. et al., *Mon. Not. Roy. Astron. Soc.* 416 (2011) 3017
 Beutler F. et al., 2012, *Mon.Not.Roy.Astron.Soc.*, **423**, 3430
 Billic N., Tupper G. B., Viollier R. D., 2002, *Phys. Lett. B*, **535**, 17
 Blake C. et al., 2012, *Mon.Not.Roy.Astron.Soc.*, **425**, 405
 Bourboux H. D. M. D et al., 2017, *Astron. Astrophys.* 608, A130
 Bourboux et al., 2017, *A&A Volume 608*, arXiv:1708.02225 [astro-ph.CO].
 Camarena D., Marra V., 2019; arXiv:1910.14125.
 Carvalho G. C. et al, 2016, *Phys. Rev. D* 93, 023530
 Carvalho G. C. et al, 2016, *Phys. Rev.*, D93, 023530
 Carvalho G. C. et al, 2016, *Phys. Rev. D* 93, 023530 (2016)
 Carvalho G. C. et al, 2017, arXiv:1709.00271 [astro-ph.CO].
 D'Amico G. et al. , 2020, *JCAP*, 05, 005, arXiv:1909.05271.
 De Carvalho E. et al., 2018, *JCAP*, 1804, 064; arXiv:1709.00113
 Di Valentino et al. 2021, *Class. Quant. Grav.*, 18 no.15, 153001.
 Dutta K. et al., 2020, *Gen.Rel.Grav.* 52 (2020) no.2, 15
 Eisenstein D. J. and Hu W., 1998, *Apj*, 496, 605
 Eisenstein D. J. et al., 2007, *ApJ*, 664, 675.
 Eisenstein D. J., Zehavi I., Hogg D. et al, 2005, *ApJ*, 633, 560
 Efstathiou G., 2021, *MNRAS*, 505, 3866
 Etherington et al., *Phil. Mag.*, 15, 761 (1933); reprinted in *GRG*, 39, 1055 (2007).
 Evslin et al., 2018, *Phys. Rev. D* 97, 103511
 Forconi M. et al., 2023, *JCAP*10 012
 Foreman-Mackey D. et al., 2013, *Publ. Astron. Soc. Pac.* 125, 306
 Fu et al., 2017, *Int.J.Mod.Phys.D* 26, 9, 1750097
 Holanda R. F. L. et al., 2012, *JCAP*06 022
 Holanda R. F. L. et al., 2016, arXiv:1611.09426
 Kable J. A. et al., 2023, *Astrophys.J.* 959 2, 143
 Lloyd Knox, Marius Millea, 2021, *Phys. Rev. D* 101, 043533
 Kourkchi E. et al, 2020, *ApJ*, 896, 3, arXiv:2004.14499.
 Lauren A. et al., 2013, *Mon.Not.Roy.Astron.Soc.*, **427**, 3435
 Lauren A. et al., 2014, *Mon.Not.Roy.Astron.Soc.*, **441**, 24
 Lemos T. et al., 2023, *Eur. Phys. J. C* 83, 495
 DOI:10.3847/1538-4357/ab4819
 Lindegren L., et al., 2020a, arXiv e-prints, p. arXiv:2012.01742
 Lindegren L., et al., 2020b, arXiv e-prints, p. arXiv:2012.03380
<https://doi.org/10.1016/j.dark.2016.06.003>
 Peebles P. J. E., Yu J. T., 1970, *ApJ*, 162, 815.
 Perlmutter S. et al., *Astrophys. J.*, **483**, 565 (1997);
 Pesce D. W. et al., 2020, *ApJL*, 891, L1
 Pietrzyński G., et al., 2019, *Nature*, 567, 200
 Reid M. J. et al., 2019, arXiv e-prints, p. *Astrophys.J.Lett.* 886 2, L27
 Ross A. J. et al, 2015, *Mon. Not. Roy. Astron. Soc.* 449, 835 (2015)
 Riess A. G. et al., 1998, *Astron. J.*, **116**, 1009
 Riess A. G. et al., 2016, *Astrophys. J.*, **826**, 56
 Riess A. G. et al., 2018, *Astrophys. J.*, **853**, 126
 Riess A. G. et al., 2018, arXiv:1804.10655 [astro-ph.CO]
 Riess A. G. et al, 2020, *ApJ*, 908, 1, arXiv:2012.08534.
 Riess A. G. et al, *Astrophys. J. Lett.* 934 (2022) L7 [2112.04510].
 Riess A. G. et al, 2021, *ApJ*, 908, L6
 Riess A. G. et al, 2019, *ApJ*, 876, 85; 1903.07603.
 Ross A. J. et al, 2015, *Mon. Not. Roy. Astron. Soc.* 449, 835
 Ruchika et al, 2022, arXiv:2306.05450
 Sánchez E. et al., 2011, *MNRAS*, 411, 277.
 Scolnic D. M., et al., 2018, *ApJ*, 859, 101; arXiv:1710.00845.
 Seo H. J., Eisenstein D.J, 2003, *ApJ*, 598, 720.
 Sunyaev R. A., Zel'dovich Ya.B., 1970, *Ap&SS*, 7, 3.
 Sutherland W., 2012, *MNRAS*, 426, 1280; arXiv:1205.0715.
 Thepsuriya K. and Lewis A., 2015, *J. Cosmology Astropart. Phys.* 2015 034 [1409.5066].
<http://dx.DOI.org/10.17909/T95Q4X>.
 Weinberg D.H. et al, 2012, *Phys. Reports*; arXiv:1201.2434.
 DOI:10.1016/j.astropartphys.2019.01.005